

MALS-NOT: IDENTIFYING RADIO-BRIGHT QUASARS FOR THE MEERKAT ABSORPTION LINE SURVEY

J.-K. KROGAGER^{1,2}, N. GUPTA³, P. NOTERDAEME¹, A. RANJAN¹, J. P. U. FYNBO⁴,
R. SRIANAND³, P. PETITJEAN¹, F. COMBES⁵, A. MAHABAL⁶

¹Institut d’Astrophysique de Paris, CNRS-UPMC, UMR7095, 98bis bd Arago, 75014 Paris, France

²Dark Cosmology Centre, Niels Bohr Institute, University of Copenhagen, Juliane Maries Vej 30, 2100 Copenhagen Ø, Denmark

³Inter-University Centre for Astronomy and Astrophysics, Post Bag 4, Ganeshkhind, 411 007 Pune, India

⁴Niels Bohr Institute, University of Copenhagen, Juliane Maries Vej 30, 2100 Copenhagen Ø, Denmark

⁵Observatoire de Paris, LERMA, CNRS: UMR8112, 61 Av. de l’Observatoire, 75014, Paris, France

⁶California Institute of Technology, 1200 E. California Blvd, Pasadena, CA 91125, USA

ABSTRACT

We present a preparatory spectroscopic survey to identify radio-bright, high-redshift quasars for the MeerKAT Absorption Line Survey (MALS). The candidates have been selected on the basis of a single flux density limit at 1.4 GHz (> 200 mJy) together with mid-infrared color criteria from the *Wide-field Infrared Survey Explorer* (*WISE*). Through spectroscopic observations using the Nordic Optical Telescope, we identify 72 quasars out of 99 candidates targeted. We measure the spectroscopic redshifts based on characteristic, broad emission lines present in the spectra. Of these 72 quasars, 64 and 48 objects are at sufficiently high redshift ($z > 0.6$ and $z > 1.4$) to be used for the L-band and UHF-band spectroscopic follow-up with the Square Kilometre Array (SKA) precursor in South Africa: the MeerKAT.

Keywords: galaxies: active — quasars: general — quasars: radio bright

1. INTRODUCTION

Extragalactic H I 21-cm and OH absorption line surveys have been mostly limited to known samples of damped Ly α absorbers (DLAs) or Mg II absorbers, from which about 50 detections of H I absorption have been reported (Briggs & Wolfe 1983; Kanekar & Chengalur 2003; Kanekar et al. 2014; Gupta et al. 2009; Curran et al. 2010; Gupta et al. 2012; Srianand et al. 2012; Dutta et al. 2017). At $z > 0.1$, only 5 OH molecular systems are known; in two of these cases absorbing gas is associated with the active galactic nucleus (AGN) itself, and in the remaining three cases absorption arises from the intervening lensing galaxy (e.g., Darling 2004; Kanekar et al. 2004). These scarce detections have led to inconclusive interpretations of the cold gas evolution in galaxies. In addition these data are biased by various preselections from optical surveys.

Thanks to large absorption line surveys with upcoming Square Kilometre Array (SKA) precursors and pathfinders, i.e., the Australia Square Kilometer Array Pathfinder (Johnston et al. 2007; Allison et al. 2017, ASKAP), APERTIF (Oosterloo et al. 2009; Maccagni et al. 2017) and MeerKAT (Gibson et al. 2015; Gupta et al. 2017; Jarvis et al. 2017), the number of absorption line systems, especially sight lines through dusty ISM, at

radio wavelengths is expected to dramatically increase over next few years.

The MeerKAT radio telescope in South Africa will be the most sensitive facility at 21-cm until the completion of SKA phase-I. Using this state-of-the-art telescope, the MeerKAT absorption line survey (MALS, Gupta et al. 2017) will probe H I 21-cm absorption out to redshift $z = 1.5$ for about 1000 blind sightlines, i.e., no preselection based on optical absorption (Ly α , Mg II, etc.) is used.

The main goal of the survey is to quantify the redshift evolution of the cold gas fraction in and around galaxies out to redshift $z = 1.5$ (and out to $z = 1.8$ using OH absorption). The cold gas phase holds important clues for the regulation of the interstellar medium, and ultimately leads to the onset of star formation. At high redshift, the best way to study the cold neutral medium is through absorption studies (e.g. Srianand et al. 2005, 2012; Ledoux et al. 2015; Noterdaeme et al. 2017), since emission line studies only detect the brightest pockets of gas and therefore do not give a representative picture of the cold gas fraction through cosmic time. Furthermore, studying the cold gas using 21-cm absorption on a purely radio-selected sample overcomes one of the main limitations of optically selected samples: the possible dust-induced bias. The extent to which optically selected

quasar samples are biased against dusty (and thereby preferentially cold and metal-rich) absorption systems has been discussed extensively through the years (Pei et al. 1991; Ellison et al. 2001; Jorgenson et al. 2006; Vladilo & Péroux 2005; Pontzen & Pettini 2009; Kaplan et al. 2010; Fynbo et al. 2013; Glikman et al. 2013; Krogager et al. 2015, 2016; Murphy & Bernet 2016). Current data suggest that the average reddening from quasar absorbers is small, yet increases with metallicity, and it has been argued that the total cosmic metal density might be underestimated by up to a factor of two (Pontzen & Pettini 2009). While the issue of a dust bias is more efficiently probed in radio selected samples, previous surveys have been too small to draw firm conclusions (Ellison et al. 2005). For this reason, the MALS sample will provide a unique opportunity to study cold gas absorbers in an unbiased way.

Moreover, the MALS sample will be useful for a range of auxiliary scientific goals; The large sample of H I and OH absorbers obtained from the survey will (i) lead to tightest constraints on the fundamental constants of physics (Kanekar et al. 2005; Rahmani et al. 2012), and (ii) be ideally suited to probe the evolution of magnetic fields in disks of galaxies via Zeeman splitting or rotation measure synthesis (Farnes et al. 2014). The survey will also provide an unbiased census of H I and OH absorbers, i.e., cold gas associated with powerful AGN ($> 1024 \text{ W Hz}^{-1}$) at $0 < z < 2$ to investigate fundamental issues related to AGN evolution and feedback (Maccagni et al. 2017), and will simultaneously deliver a blind H I and OH emission line survey, and radio continuum survey. For more details about the individual science goals of MALS, we refer to the survey description (Gupta et al. 2017).

The MALS survey design is specified in Table 2 of Gupta et al. (2017). Specifically, to maximize the optical depth sensitivity and redshift coverage, the L- and UHF-band pointings will be centred at flat-spectrum radio quasars (FSRQs) at $z > 0.6$ and $z > 1.4$, respectively. Bright FSRQs with known spectroscopic redshifts, especially in the southern hemisphere, are rare; Therefore, we have initiated a large campaign to identify more high-redshift, radio-bright quasars using infrared color criteria to limit the influence of dust. The infrared-selected radio quasar candidates are then followed up using optical spectroscopy to classify the nature of the source and to measure its redshift. For the spectroscopic observations, higher priority is given to candidates that are likely to be FSRQs. Due to the large number of targets needed to be identified, the task has been split among several observing facilities, and in this paper, we report on one part of the survey carried out at the Nordic Optical Telescope (NOT) at the Observatorio del Roque de los Muchachos on La Palma, Spain, from which we can

access the most northern targets of the overall survey. The results from the Southern African Large Telescope (SALT) campaign will be presented in a future paper. The MeerKAT observing campaign is expected to start in 2018 and the survey will be carried out over a period of 5 years.

The paper is structured as follows. In Section 2, we present the target selection criteria; in Section 3, we describe the optical follow-up and the data processing; in Section 4, we present the results; and in Section 5, we provide a short discussion of caveats and a summary of our findings.

2. TARGET SELECTION

First step was to assemble a catalog of southern ($\delta < +20 \text{ deg}$) radio sources that are bright enough ($> 200 \text{ mJy}$) to meet the requirements of MALS in 1–2 hrs of telescope integration time. For this purpose, we used the NRAO VLA Sky Survey (NVSS; Condon et al. 1998) at 1.4 GHz and the Sydney University Molonglo Sky Survey (SUMSS; Bock et al. 1999; Mauch et al. 2003) at 843 MHz¹. The radio source catalog was then cross-correlated with photometry from the *Wide-field Infrared Survey Explorer* [WISE, Wright et al. 2010]. The WISE photometry covers 4 bands, here designated as W_1 ($3.4 \mu\text{m}$), W_2 ($4.6 \mu\text{m}$), W_3 ($12 \mu\text{m}$), and W_4 ($22 \mu\text{m}$). The cross-matching is performed on the coordinates using a matching radius of 2 arcsec which corresponds to the astrometric uncertainty of the radio sources. The WISE color-space for radio sources identified as quasars from the Sloan Digital Sky Survey (SDSS, York et al. 2000) spectroscopic catalog is shown in Fig. 2. The color-coding of each bin in the color-color diagram shows the average redshift of sources in the given bin. It is clearly seen that low-redshift quasars tend to cluster in one part of this color-space and we can therefore limit the number of low-redshift interlopers by applying the following photometric cuts (similar to fig. 1 of Krogager et al. 2016):

$$W_1 - W_2 < 1.3 \times (W_2 - W_3) - 3.04$$

and

$$W_1 - W_2 > 0.6 .$$

The lower limit on the $W_1 - W_2$ color is imposed to limit the number of stars and galaxies in our sample, since the contamination fraction increases rapidly when expanding to lower values of $W_1 - W_2$ (e.g., Stern et al. 2012; Richards et al. 2015). Stern et al. (2012) estimate the purity of quasars with $W_1 - W_2 > 0.6$ to be $\sim 70\%$.

¹ A spectral index of 0.8 was assumed to determine 1.4 GHz flux densities of targets from SUMSS.

For the NOT observations we limited the observations to northern targets, i.e., $-20^\circ < \delta < +20^\circ$. This resulted in a parent sample of 196 targets. Objects with compact radio morphology and flat spectral shapes are given priority as these are likely to be compact at cm-wavelengths and hence preferred for the intervening absorption studies (Gupta et al. 2012). In total we reject 41 targets with complex or extended radio morphologies based on available arcsec scale L-band images in FIRST (Becker et al. 1995).

Furthermore, 14 sources are discarded based on extended optical morphology (classified as galaxy in SDSS) as these are dominated by low-redshift ($z < 1.4$) sources². Five sources are discarded due to overlap with the plane of the Milky Way (closer than ± 15 deg Galactic latitude) to minimize the contamination from stars. We exclude two sources since they are bright stars based on the finding charts, three sources have been excluded since spectroscopic redshifts from SDSS are already available, and one source is excluded due to a catalog error, which was not discovered until after the observing runs. The final sample of candidates is thus made up of 130 targets.

3. OBSERVATIONS AND DATA PROCESSING

During two observing runs in August 2016 (P53-012) and February 2017 (P54-005), we have observed a total of 99 candidate quasars with the (NOT) using the Andalucía faint object spectrograph and camera (ALFOSC). For all observations, we binned the CCD pixels by a factor of 2 along the wavelength axis and we aligned the slit with the parallactic angle. The candidates were observed using grism #4 which covers the wavelength range from about 3200 Å to 9100 Å at a resolution of about $R \sim 300$ (depending on the slit-width used). During the observations we matched the slit-width according the seeing in order to limit slit-losses. No blocking filter was used for the observations to maximize throughput. We thus caution, that the spectra suffer from second order contamination effects. However, as our main purpose of the spectroscopic follow-up was merely to secure the classification and to measure redshifts, the second order contamination is not of great importance. The exposure time and slit-width used for the observation of each target is summarized in Table 1. The seeing varied quite significantly in the Feb run ranging from 0.5 arcsec in the best case to >2 arcsec in the worst case. For the Aug run, the seeing was more stable around ~ 1

² During the first night of observations we observed 8 sources with extended morphology and only 1 was a $z > 1.4$ quasar, and the morphological classification of this source is most likely affected by a very bright nearby star.

arcsec. Photometric properties for the observed sample are summarized in Table A1 in Appendix A.

During the observations, we gave priority to targets with a visible optical counterpart in the finding chart or sources that had optical data available, such as SDSS photometry. This allowed us to identify an optical counterpart in acquisition images of typically 10-20 seconds, reaching depths of $R \sim 21$ mag. In total, 40 targets had no visible counterpart in the finding charts. Since the finding charts were based on rather shallow photometry from the Digitized Sky Survey, we also attempted to look for optical counterparts where no obvious sources were visible in the finding charts by making deeper (1 minute, reaching $R \sim 22.5$ mag) acquisition images centred on the radio position. The results from these blind positions are summarized in Sect. 4.

We used He and Ne calibration lamps for the wavelength calibration and on each night we observed at least one spectroscopic standard star in order to calibrate the response of the instrument.

Firstly, the raw frames were bias subtracted and flat-field corrected using Halogen lamp flats. The background was then subtracted row by row (the spectra were dispersed vertically on the CCD) using a low order Chebyshev polynomial fit with robust sigma-clipping. Cosmic rays were rejected using the method developed by van Dokkum (2001). We use the Python implementation, `astroscrappy`³, which is significantly faster than the original implementation in IRAF⁴.

Extraction and calibration of the 1-dimensional (1D) spectra was performed using the IRAF tasks `apall`, `identify`, `sensitivity`, and `calibrate`. The respective vacuum wavelength solutions and sensitivity functions were applied to the 2D spectral frames in order to obtain calibrated 2D spectra.

³ Written by Curtis McCully, see documentation on GitHub: <https://github.com/astropy/astroscrappy>

⁴ IRAF is distributed by the National Optical Astronomy Observatory, which is operated by the Association of Universities for Research in Astronomy (AURA) under cooperative agreement with the National Science Foundation.

Table 1. Overview of spectroscopic sample

Target	R.A.	Decl.	F _{1.4GHz} (mJy)	Exp. time (sec)	Slit width (arcsec)	z_{spec}	Classification
MALS0017–1256	00:17:08.03	−12:56:24.9	929.7	300	1.0	0.870	Quasar
MALS0022+0608	00:22:32.46	+06:08:04.6	339.7	120	1.3	—	Blazar?
MALS0042+1246	00:42:43.06	+12:46:57.6	635.0	360	1.3	2.150	Quasar
MALS0051+1747	00:51:47.15	+17:47:10.3	1367.5	480	1.3	0	Galaxy
MALS0053–0702	00:53:15.65	−07:02:33.4	248.2	450	1.0	2.130	Quasar
MALS0105+1845	01:05:49.69	+18:45:07.1	339.5	600	1.0	—	Blazar?
MALS0117–0425	01:17:27.84	−04:25:11.5	421.4	1200	1.0	1.720	Quasar
MALS0211+1707	02:11:48.77	+17:07:23.2	539.8	600	1.3	1.980	Quasar
MALS0216+1724	02:16:50.70	+17:24:04.9	395.2	300	1.3	1.530	Quasar
MALS0226+0937	02:26:13.72	+09:37:26.3	374.6	60	1.3	2.610	Quasar
MALS0226+1941	02:26:39.92	+19:41:10.1	209.8	900	1.0	2.190	Quasar
MALS0240+0832	02:40:46.80	+08:32:58.3	305.4	300	1.3	1.100	Quasar
MALS0249+0440	02:49:39.93	+04:40:28.9	420.5	420	1.3	2.010	Quasar
MALS0249+1237	02:49:44.50	+12:37:06.3	261.2	300	1.3	0	Star/galaxy
MALS0256–0218	02:56:30.36	−02:18:44.5	260.3	300	1.0	1.970	Quasar
MALS0304–1126	03:04:13.80	−11:26:53.5	335.0	1200	1.0	1.550	Quasar
MALS0314–0909	03:14:07.94	−09:09:46.9	226.8	1200	1.0	0.312	Emission line galaxy
MALS0317+0655	03:17:06.76	+06:55:50.3	211.8	1800	1.3	0.275	Quasar
MALS0328–0152	03:28:08.59	−01:52:20.2	221.9	600	1.0	2.681	Quasar
MALS0341+1519	03:41:57.75	+15:19:25.5	200.4	2700	1.0	1.699	Quasar, blind observation
MALS0350–0351	03:50:16.86	−03:51:11.3	230.5	600	1.0	0.611	Quasar
MALS0356+1900	03:56:33.46	+19:00:34.6	1051.3	420	1.0	1.480	Quasar
MALS0356–0831	03:56:34.55	−08:31:21.3	239.7	1800	1.0	1.447	Quasar
MALS0455+1850	04:55:41.91	+18:50:10.9	328.1	1500	1.0	0.548	Quasar
MALS0510–1959	05:10:24.23	−19:59:50.3	336.2	1200	1.0	0.472	Quasar
MALS0512+1517	05:12:40.99	+15:17:23.8	966.5	600	1.0	2.568	Quasar
MALS0516+0732	05:16:56.35	+07:32:52.7	231.7	600	1.0	2.594	Quasar
MALS0519+1746	05:19:38.34	+17:46:41.2	319.1	1200	1.0	0	Galaxy, early type
MALS0529–1126	05:29:05.55	−11:26:07.5	455.8	900	1.0	0.995	Quasar
MALS0600–0710	06:00:12.92	−07:10:37.9	224.9	1800	1.0	0	Galaxy/Star
MALS0730+1739	07:30:37.09	+17:39:51.5	694.2	3600	1.0	—	N/A, blind observation
MALS0731+1433	07:31:59.01	+14:33:36.3	316.5	300	1.0	2.632	Quasar
MALS0824–1029	08:24:44.81	−10:29:43.6	345.4	300	1.0	0	Post-starburst Galaxy
MALS0836+0406	08:36:01.35	+04:06:36.0	435.3	3600	1.0	0.743	Galaxy, late type, blind observation
MALS0909–1637	09:09:10.66	−16:37:53.8	340.1	1800	1.0	2.471	Quasar
MALS0909–0500	09:09:16.99	−05:00:53.2	457.2	1500	1.0	0.403	Galaxy, late type
MALS0910–0526	09:10:51.01	−05:26:26.8	337.9	300	1.0	2.387	Quasar
MALS0939–1731	09:39:19.21	−17:31:35.4	263.3	600	1.0	1.831	Quasar
MALS0941–0321	09:41:46.01	−03:21:21.7	346.2	1800	1.0	1.849	Quasar

Table 1 continued

Table 1 (*continued*)

Target	R.A.	Decl.	F _{1.4GHz} (mJy)	Exp. time (sec)	Slit width (arcsec)	<i>z</i> _{spec}	Classification
MALS0951–0601	09:51:38.34	−06:01:38.0	378.8	600	1.0	1.839	Quasar
MALS1007–1817	10:07:43.51	−18:17:32.4	205.2	900	1.0	0.493	Galaxy, late type
MALS1008–0959	10:08:02.27	−09:59:19.3	645.3	600	1.0	1.688	Quasar
MALS1009+1602	10:09:54.53	+16:02:03.8	201.9	900	1.0	1.770	Quasar - redshift tentative
MALS1024–0852	10:24:44.61	−08:52:06.4	463.8	3600	1.3	0.468	Emission line galaxy, blind observation
MALS1033–1210	10:33:35.61	−12:10:32.1	2065.1	900	1.0	1.328	Emission line galaxy
MALS1043+1641	10:43:47.34	+16:41:06.9	259.1	1800	1.0	0.399	Galaxy, late type
MALS1046+1535	10:46:08.12	+15:35:36.6	430.9	3600	1.0	—	N/A, blind observation
MALS1050–0318	10:50:24.43	−03:18:08.8	243.5	420	1.0	1.806	Quasar
MALS1059–1118	10:59:55.36	−11:18:18.7	314.5	900	1.0	1.942	Quasar
MALS1119–0527	11:19:17.36	−05:27:07.9	1174.4	600	1.0	2.651	Quasar
MALS1124–1501	11:24:02.56	−15:01:59.1	261.9	600	1.0	2.551	Quasar
MALS1148+1404	11:48:25.45	+14:04:49.7	322.0	4000	1.0	0.727	Emission line galaxy, blind observation
MALS1150+1317	11:50:43.70	+13:17:36.1	254.4	600	1.0	1.530	Quasar
MALS1206–0714	12:06:32.23	−07:14:52.6	698.8	2400	1.3	2.263	Quasar
MALS1215–0628	12:15:14.42	−06:28:03.5	360.4	1800	1.8	3.223	Quasar
MALS1218–0631	12:18:36.18	−06:31:15.8	409.1	1200	1.8	0.658	Quasar
MALS1219–1809	12:19:05.45	−18:09:11.2	300.3	600	1.0	0.189	Quasar
MALS1221–1237	12:21:23.49	−12:37:24.1	343.7	1800	1.8	1.882	Quasar
MALS1225–1144	12:25:24.48	−11:44:31.2	479.5	2700	1.0	—	N/A, blind observation
MALS1231–1236	12:31:50.30	−12:36:37.5	276.0	1200	1.8	2.100	Quasar
MALS1318–1441	13:18:56.01	−14:41:55.0	283.0	2000	1.8	0.632	Quasar
MALS1343–0834	13:43:09.26	−08:34:57.5	241.5	720	1.0	1.077	Quasar
MALS1351–1019	13:51:31.98	−10:19:32.9	726.1	1500	1.8	2.998	Quasar
MALS1456+0456	14:56:25.83	+04:56:45.2	287.9	1200	1.0	2.136	Quasar
MALS1623+1239	16:23:03.03	+12:39:58.4	523.3	300	1.0	0	Star/Galaxy
MALS1625–0416	16:25:39.34	−04:16:16.3	257.2	1200	1.0	0	Galaxy, early type
MALS1639+1144	16:39:06.46	+11:44:09.2	341.9	900	1.0	0	Star/Galaxy
MALS1645–0432	16:45:52.10	−04:32:53.3	423.3	1800	1.0	—	N/A
MALS1649+0626	16:49:50.51	+06:26:53.3	389.2	300	1.0	2.130	Quasar
MALS1650–1248	16:50:38.03	−12:48:54.5	275.5	720	1.0	2.490	Quasar
MALS1653–0102	16:53:57.67	−01:02:14.2	317.4	600	1.0	1.070	Quasar
MALS1716–0613	17:16:27.09	−06:13:56.5	229.9	480	1.0	1.840	Quasar
MALS1721+1626	17:21:05.79	+16:26:49.1	507.9	900	1.0	1.814	Quasar
MALS1722+1652	17:22:39.45	+16:52:08.7	257.1	600	1.0	—	N/A
MALS1724+0326	17:24:23.07	+03:26:32.5	217.8	450	1.3	0	Galaxy
MALS1725+0622	17:25:07.45	+06:22:42.1	213.4	180	1.0	1.330	Quasar
MALS2034–0523	20:34:25.65	−05:23:32.2	419.7	900	1.3	2.070	Quasar
MALS2054–0932	20:54:56.08	−09:32:40.8	313.6	600	1.0	1.350	Quasar
MALS2059–1440	20:59:59.61	−14:40:43.1	1018.1	1500	1.3	0.690	Galaxy
MALS2120+1327	21:20:42.48	+13:27:24.2	401.5	600	1.3	1.110	Quasar

Table 1 continued

Table 1 (*continued*)

Target	R.A.	Decl.	F _{1.4GHz} (mJy)	Exp. time (sec)	Slit width (arcsec)	z_{spec}	Classification
MALS2139+1718	21:39:37.03	+17:18:26.9	219.4	360	1.3	1.700	Quasar
MALS2158+0925	21:58:00.88	+09:25:46.4	437.7	600	1.3	0.445	Quasar
MALS2201+0312	22:01:27.50	+03:12:15.6	300.5	900	1.3	2.190	Quasar
MALS2220+1307	22:20:04.97	+13:07:12.1	812.0	1800	1.3	0.760	Quasar
MALS2223+1213	22:23:59.11	+12:13:38.9	246.4	1080	1.0	0	Galaxy
MALS2224+1304	22:24:20.03	+13:04:50.2	294.5	1800	1.3	0.685	Quasar
MALS2230+0348	22:30:50.19	+03:48:36.8	242.8	3600	1.3	1.330	Quasar, blind observation
MALS2238-1344	22:38:26.48	-13:44:22.6	241.2	600	1.3	0.257	Quasar
MALS2243+1814	22:43:54.81	+18:14:45.9	1004.4	480	1.0	0.760	Quasar
MALS2247+1211	22:47:05.52	+12:11:51.4	223.7	1800	1.0	2.185	Quasar
MALS2300+1940	23:00:36.41	+19:40:02.9	210.4	360	1.3	2.160	Quasar
MALS2300+0337	23:00:40.87	+03:37:10.3	509.0	600	1.3	1.860	Quasar
MALS2308-1149	23:08:05.25	-11:49:45.7	256.8	1500	1.0	1.940	Quasar
MALS2310+1114	23:10:02.89	+11:14:03.6	248.1	360	1.3	1.550	Quasar
MALS2316+0429	23:16:34.61	+04:29:40.2	214.0	480	1.0	2.160	Quasar
MALS2332-1423	23:32:31.61	-14:23:18.8	234.1	1500	1.0	0.524	Quasar
MALS2338-1218	23:38:08.04	-12:18:51.4	450.9	600	1.0	1.185	Quasar
MALS2340+0959	23:40:07.26	+09:59:59.0	205.0	4500	1.3	2.210	Quasar, blind observation
MALS2359+1924	23:59:14.02	+19:24:20.6	284.1	1800	1.0	0.515	Quasar
MALS0845-1118	08:45:48.34	-11:18:00.1	264.4	—	—	—	No source in acquisition image.
MALS0954+1252	09:54:14.75	+12:52:22.6	355.7	—	—	—	No source in acquisition image.
MALS1130-1006	11:30:15.25	-10:06:38.4	215.2	—	—	—	No source in acquisition image.
MALS2258-0958	22:58:13.47	-09:58:17.2	225.7	—	—	—	No source in acquisition image.

4. RESULTS

We classify each observed target based on spectral features in the extracted 1D spectra. In most cases quasars are easily identified due to their broad emission lines, which furthermore enable us to measure its redshift. The summary of all classifications and the measured redshifts are given in Table 1. The uncertainty on the spectroscopic redshift is of the order $\sigma_z = 0.005$. In cases where there are only narrow emission lines, we classify the target as an emission line galaxy and provide the measured redshift. In 8 cases we were not able to obtain a secure classification. These are marked either as unknown identification ('N/A'), blazar or tentative (redshift followed by ':') in Table 1. In total, we securely identify 72 quasars out of 99 observed targets, and 48 of these are at a sufficiently high redshift ($z > 1.4$) for the UHF band spectroscopic observations of the MALS survey. For the L-band observations of MALS 64 out of the

72 quasars are at sufficiently high redshifts ($z > 0.6$). In Fig. 1, we show the distribution of spectroscopic redshifts for all objects where it was possible to determine the redshift. All targets are shown in the *WISE* color-color plot in Fig. 2. The distribution of redshifts in the mid-infrared color-space follows largely the same pattern as the underlying SDSS sample taking into account the large scatter in the redshifts (± 0.8) for each bin in color-space. In accordance with previous studies of quasars in the near-infrared color-space (e.g., Assef et al. 2010; Stern et al. 2012), we find that the fraction of contaminants decreases for increasing $W_1 - W_2$ color. A preview of the spectra are shown in Figs. A1 and A2 in Appendix A (the full sets of figures are available online).

As mentioned in Sect. 3, we attempted to identify optical counterparts for 13 targets where no source was visible in the shallow finding chart. After a long acquisition image (typically 1 min), we were able to

identify a faint source at the position of the radio source in 9 out of 13 cases. Out of these 9 blind observations, we were able to identify three quasars and three galaxies; three spectra did not result in any identification. These 9 blind observations are marked as ‘blind observation’ in the classification notes of Table 1. In the last 4 out of the 13 blind fields, we did not observe any optical counterpart in the deeper acquisition images and hence did not proceed with the spectroscopic observations. These are listed in the bottom part of Table 1 for completeness, but they are not counted as actual spectroscopic observations in this optical follow-up study. In order not to bias our survey, these unidentified radio sources will be part of our full spectroscopic campaign to search for H I and OH absorption at radio wavelengths.

We searched the spectra for absorption lines either from the quasar host or from intervening systems. The objects with clearly visible absorption features are given in Table 2. In cases where we were able to identify the lines, we also give the absorber redshift. We note that due to the low resolution and limited signal-to-noise ratio in the continuum, the identifications are tentative in most cases.

Table 2. Absorption Systems

Target	z_{abs}	Notes
MALS0053–0702	...	No ID
MALS0117–0425	1.315	Mg II
MALS0226+0937	...	No ID
MALS0226+1941	2.036	Mg II
MALS0256–0218	1.970	BAL
MALS0328–0152	...	No ID
MALS0512+1517	2.568	Associated absorber
MALS0516+0732	2.594	Associated absorber
MALS0939–1731	1.319	Mg II
—	0.739	Mg II
MALS1351–1019	2.758	Ly α
MALS1649+0626	2.310	Associated absorber
MALS1716–0613	1.661	Mg II
MALS2139+1718	1.326	Mg II
MALS2247+1211	2.185	Associated absorber
MALS2340+0959	...	No ID

5. DISCUSSION AND SUMMARY

Using strong, broad emission lines as the only indicator for quasar identification is a simple and robust way

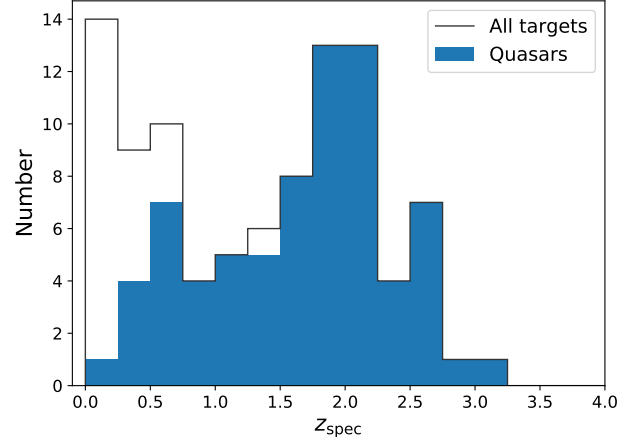


Figure 1. Redshift distribution of spectroscopically observed targets.

to verify that the source is indeed a quasar and simultaneously allows a determination of the redshift. However, this approach comes with one main drawback: Not all quasars exhibit these broad, characteristic emission lines (Meusinger et al. 2012, 2016; Krogager et al. 2015, 2016). For the main science case of the MALS project, namely the study of intervening cold gas absorption, such a bias against non-standard quasars (incl. type-II and blazars) will have no significant implications since the bias is intrinsic to the quasars and not caused by the intervening absorbers. However, for the science case related to AGN fuelling and intrinsic properties of the AGN, the bias must be kept in mind.

From our observations at the NOT we can estimate the severeness of the bias from the number of unidentified spectra in our survey. In total, we found 8 targets with no clear identification and 72 quasars. As a conservative estimate, assuming that all unidentified sources are indeed atypical quasars without broad emission lines, we thus find a maximal missing fraction of 10%.

The fraction of quasars in this region of *WISE* color space has independently been estimated at around 70% (Stern et al. 2012), which agrees well with the observed number of quasars (72 out of 99). This indicates that the missing number of quasars is indeed small.

We note that some targets are classified as tentative blazars or atypical quasars, but for these targets we lack spectral features that allow us to determine the redshift. Thus, for the purpose of MALS, these targets are of little interest.

In summary, we have carried out a spectroscopic survey for radio loud quasars at high redshift. We used a single flux density limit at 1.4 GHz (requiring that candidates have $F_{1.4\text{GHz}} > 200 \text{ mJy}$) together with simple color criteria in the $W_1 - W_2$ and $W_2 - W_3$ color-space

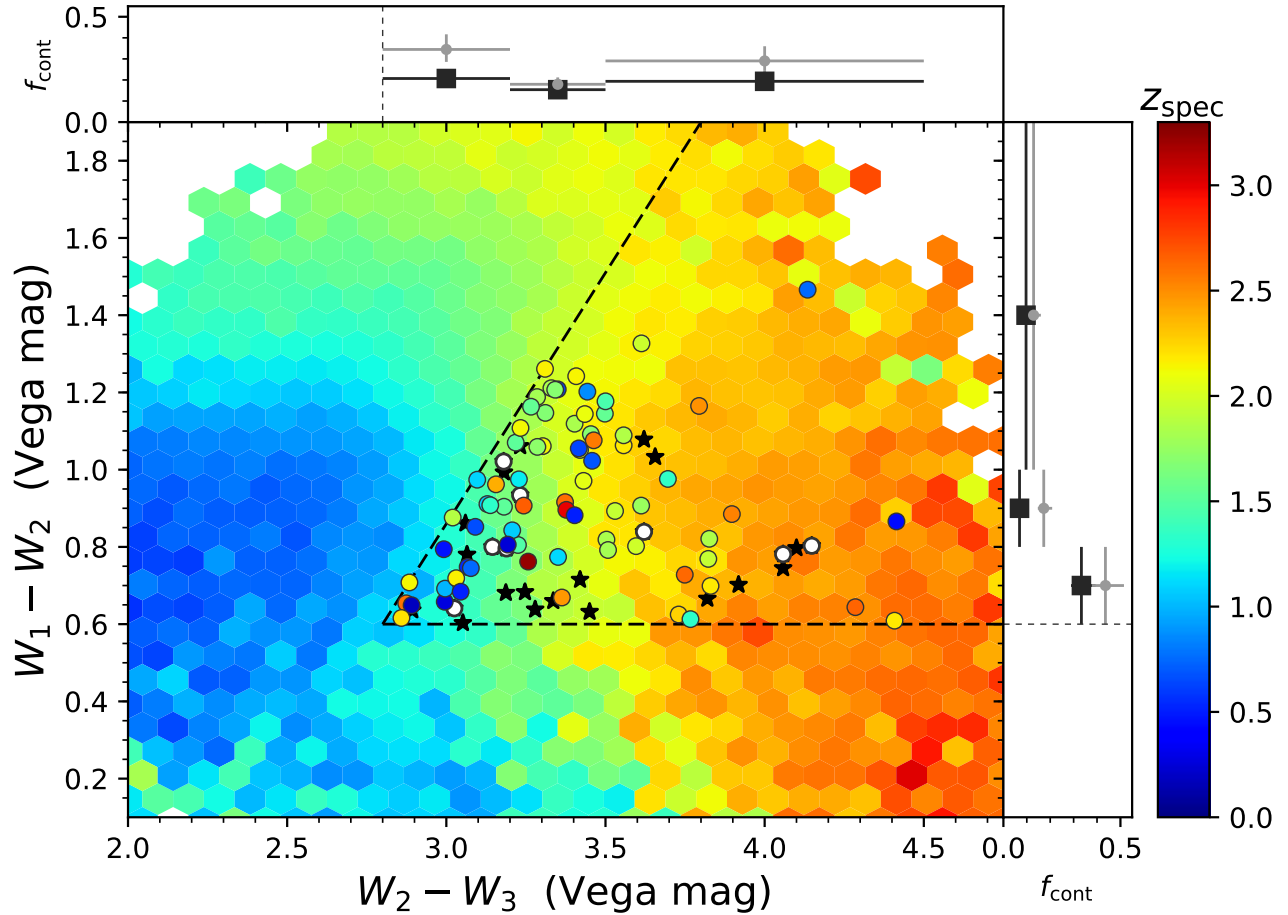


Figure 2. *WISE* color-color plot for quasars. The underlying distribution shows spectroscopically observed quasars from the Sloan Digital Sky Survey (Pâris et al. 2017). The color coding corresponds to the mean redshift of quasars in a given bin. The MALS quasars are shown as large, colored dots (following the same color coding). Black stars indicates contaminating stars or galaxies and white dots mark the candidates for which no classification was possible. The dashed lines show the region of color-space that we used to select high-redshift candidates. The two panels at the top and right edges indicate the contaminating fraction, f_{cont} , of stars and galaxies in dark gray, and the contamination including the unidentified sources is shown in light gray.

to select candidates at $z > 1.5$. Using the NOT we have carried out a survey of 99 candidates with compact radio morphologies. Out of the total number of candidates observed, 72 are quasars of which 64 and 48 objects are at sufficiently high redshift for the L- and UHF-band spectroscopic observations as part of MALS.

JKK acknowledges financial support from the Danish Council for Independent Research (EU-FP7 under the Marie-Curie grant agreement no. 600207) with reference DFF-MOBILEX-5051-00115. AR, NG, RS, PN and PPJ acknowledge the support from Indo-French Centre for the Promotion of Advance Research (IFCPAR) under project number 5504-2. Based on observations made with the Nordic Optical Telescope, operated on the island of La Palma jointly by Denmark, Finland, Iceland, Norway, and Sweden, in the Spanish Observatorio del Roque de los Muchachos of the Insti-

tuto de Astrofísica de Canarias. The Digitized Sky Survey is based on photographic data obtained using The UK Schmidt Telescope. The UK Schmidt Telescope was operated by the Royal Observatory Edinburgh, with funding from the UK Science and Engineering Research Council, until 1988 June, and thereafter by the Anglo-Australian Observatory. Original plate material is copyright Âl the Royal Observatory Edinburgh and the Anglo-Australian Observatory. The plates were processed into the present compressed digital form with their permission. The Digitized Sky Survey was produced at the Space Telescope Science Institute under US Government grant NAG W-2166.

REFERENCES

- Allison, J. R., Moss, V. A., Macquart, J.-P., et al. 2017, MNRAS, 465, 4450
- Assef, R. J., Kochanek, C. S., Brodwin, M., et al. 2010, ApJ, 713, 970
- Becker, R. H., White, R. L., & Helfand, D. J. 1995, ApJ, 450, 559
- Bock, D. C.-J., Large, M. I., & Sadler, E. M. 1999, AJ, 117, 1578
- Briggs, F. H., & Wolfe, A. M. 1983, ApJ, 268, 76
- Condon, J. J., Cotton, W. D., Greisen, E. W., et al. 1998, AJ, 115, 1693
- Curran, S. J., Tzanavaris, P., Darling, J. K., et al. 2010, MNRAS, 402, 35
- Darling, J. 2004, ApJ, 612, 58
- Dutta, R., Srianand, R., Gupta, N., et al. 2017, MNRAS, 465, 4249
- Ellison, S. L., Hall, P. B., & Lira, P. 2005, AJ, 130, 1345
- Ellison, S. L., Yan, L., Hook, I. M., et al. 2001, A&A, 379, 393
- Farnes, J. S., O'Sullivan, S. P., Corrigan, M. E., & Gaensler, B. M. 2014, ApJ, 795, 63
- Fynbo, J. P. U., Krogager, J.-K., Venemans, B., et al. 2013, ApJS, 204, 6
- Gibbon, T. B., Rotich Kipnoo, E. K., Gamatham, R. R. G., et al. 2015, Journal of Astronomical Telescopes, Instruments, and Systems, 1, 028001
- Glikman, E., Urrutia, T., Lacy, M., et al. 2013, ApJ, 778, 127
- Gupta, N., Srianand, R., Petitjean, P., et al. 2012, A&A, 544, A21
- Gupta, N., Srianand, R., Petitjean, P., Noterdaeme, P., & Saikia, D. J. 2009, MNRAS, 398, 201
- Gupta, N., Srianand, R., Baan, W., et al. 2017, ArXiv e-prints, arXiv:1708.07371
- Jarvis, M. J., Taylor, A. R., Agudo, I., et al. 2017, ArXiv e-prints, arXiv:1709.01901
- Johnston, S., Bailes, M., Bartel, N., et al. 2007, PASA, 24, 174
- Jorgenson, R. A., Wolfe, A. M., Prochaska, J. X., et al. 2006, ApJ, 646, 730
- Kanekar, N., & Chengalur, J. N. 2003, A&A, 399, 857
- Kanekar, N., Chengalur, J. N., & Ghosh, T. 2004, Physical Review Letters, 93, 051302
- Kanekar, N., Carilli, C. L., Langston, G. I., et al. 2005, Physical Review Letters, 95, 261301
- Kanekar, N., Prochaska, J. X., Smette, A., et al. 2014, MNRAS, 438, 2131
- Kaplan, K. F., Prochaska, J. X., Herbert-Fort, S., Ellison, S. L., & Dessauges-Zavadsky, M. 2010, PASP, 122, 619
- Krogager, J.-K., Geier, S., Fynbo, J. P. U., et al. 2015, ApJS, 217, 5
- Krogager, J.-K., Fynbo, J. P. U., Heintz, K. E., et al. 2016, ApJ, 832, 49
- Ledoux, C., Noterdaeme, P., Petitjean, P., & Srianand, R. 2015, A&A, 580, A8
- Maccagni, F. M., Morganti, R., Oosterloo, T. A., Geréb, K., & Maddox, N. 2017, A&A, 604, A43
- Mauch, T., Murphy, T., Butterly, H. J., et al. 2003, MNRAS, 342, 1117
- Meusinger, H., Schalldach, P., Mirhosseini, A., & Pertermann, F. 2016, A&A, 587, A83
- Meusinger, H., Schalldach, P., Scholz, R.-D., et al. 2012, A&A, 541, A77
- Murphy, M. T., & Bernet, M. L. 2016, MNRAS, 455, 1043
- Noterdaeme, P., Krogager, J.-K., Balashev, S., et al. 2017, A&A, 597, A82
- Oosterloo, T., Verheijen, M. A. W., van Cappellen, W., et al. 2009, in proceedings of science, Wide Field Astronomy & Technology for the Square Kilometre Array, PoS(SKADS2009)070
- Pâris, I., Petitjean, P., Ross, N. P., et al. 2017, A&A, 597, A79
- Pei, Y. C., Fall, S. M., & Bechtold, J. 1991, ApJ, 378, 6
- Pontzen, A., & Pettini, M. 2009, MNRAS, 393, 557
- Rahmani, H., Srianand, R., Gupta, N., et al. 2012, MNRAS, 425, 556
- Richards, G. T., Myers, A. D., Peters, C. M., et al. 2015, ApJS, 219, 39
- Srianand, R., Gupta, N., Petitjean, P., et al. 2012, MNRAS, 421, 651
- Srianand, R., Petitjean, P., Ledoux, C., Ferland, G., & Shaw, G. 2005, MNRAS, 362, 549
- Stern, D., Assef, R. J., Benford, D. J., et al. 2012, ApJ, 753, 30
- van Dokkum, P. G. 2001, PASP, 113, 1420
- Vladilo, G., & Péroux, C. 2005, A&A, 444, 461
- Wright, E. L., Eisenhardt, P. R. M., Mainzer, A. K., et al. 2010, AJ, 140, 1868
- York, D. G., Adelman, J., Anderson, Jr., J. E., et al. 2000, AJ, 120, 1579

APPENDIX

A. SUPPORTING FIGURES AND TABLES

For each 1D spectrum in Fig. A1, we show the extracted data in black and the associated emission lines are marked if a spectroscopic redshift has been determined (as indicated in the upper right corner). If not, then we give $z = -1$ in the upper right corner. The 2D spectra in Fig. A2 are shown with a linear color-scale matched to the noise level in each spectrum; specifically we use the median absolute deviation (MAD) to estimate the background noise and set the lower scale to $-1 \times \text{MAD}$ and the upper scale to $+6 \times \text{MAD}$. Above each 2D spectrum we give the target name and the observing period (P53-012 or P54-005) in which the spectrum was obtained.

In Table A1, we summarize the photometric properties of the spectroscopic sample compiling the radio brightness at 1.4 GHz, optical g and r band magnitudes from SDSS together with our rough estimate of the r -band magnitude from the observed spectrum. We note that the synthetic r -band magnitudes have not been corrected for possible slit losses and their typical uncertainties are of the order of 0.2 mag. Lastly, we include mid-infrared photometry and colors from *WISE*.

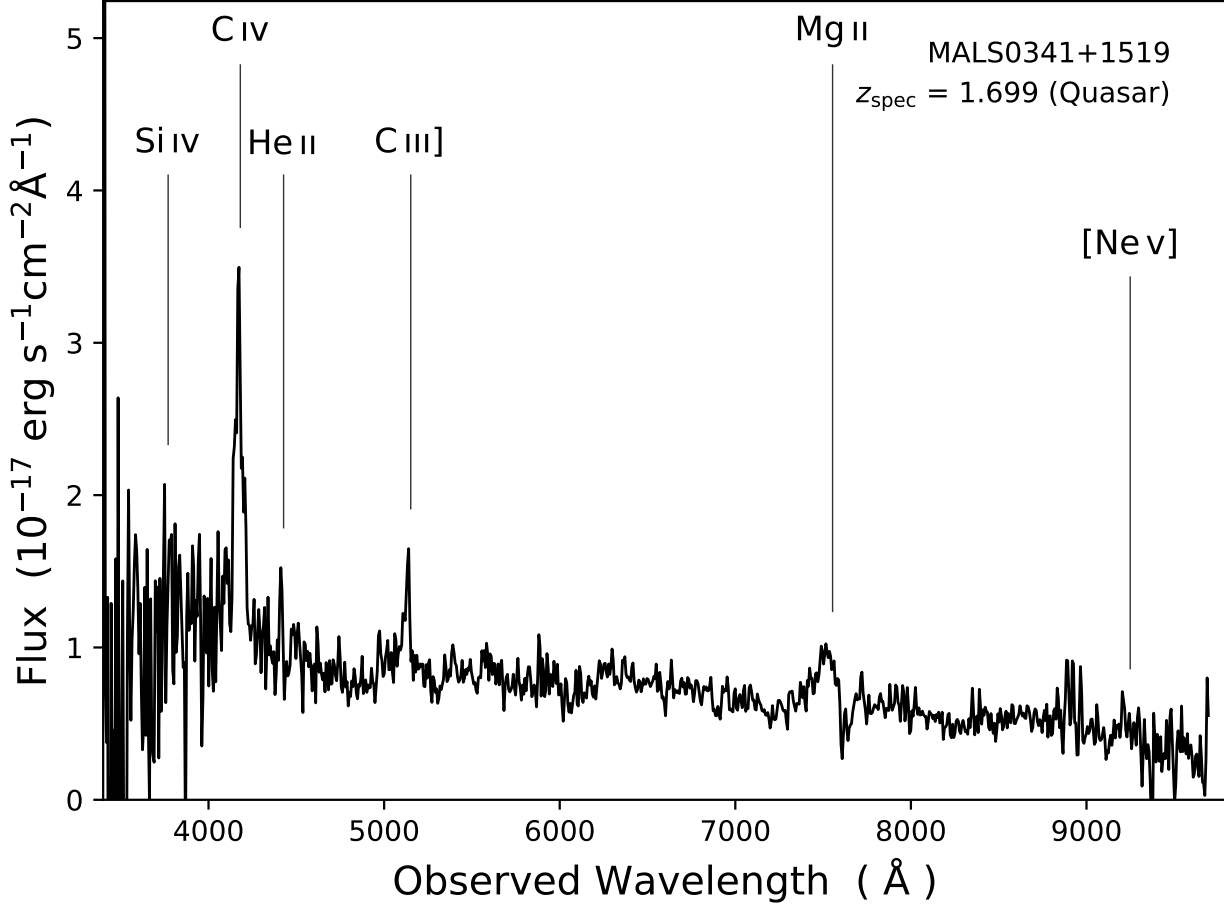


Figure A1. Extracted 1-dimensional spectrum from the NOT. The location of various emission lines typically present in quasar spectra are shown for the redshift given in the upper right corner. A redshift of $z_{\text{spec}} = -1$ means that no spectroscopic identification was possible, and a redshift of $z_{\text{spec}} = 0$ means that the target is classified as a star or galaxy with no emission features.

(The complete figure set (99 images) is available in the online journal and in the source files.)

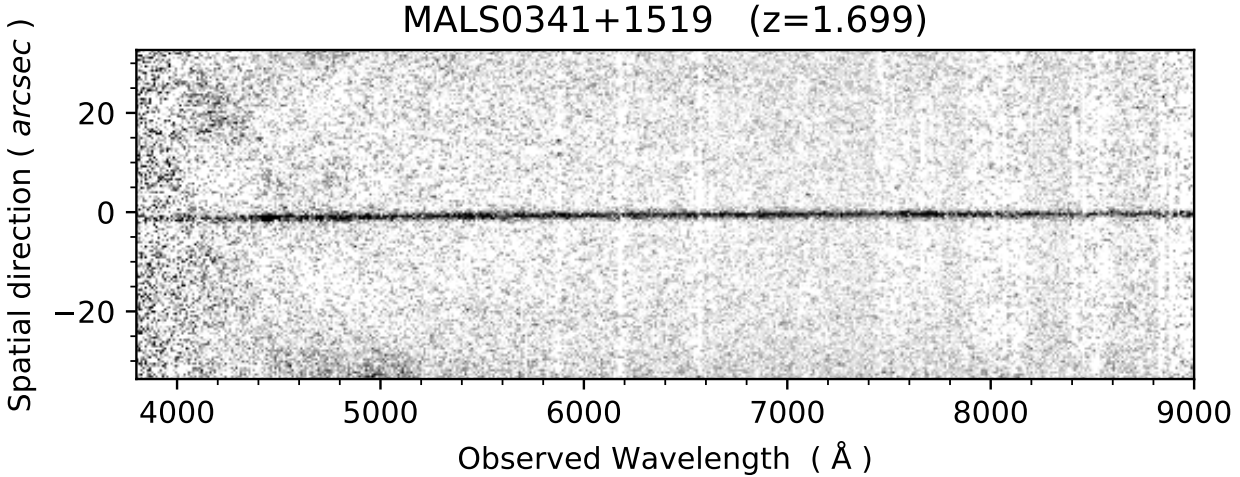


Figure A2. Processed 2-dimensional spectrum. (The complete figure set (99 images) is available in the online journal and in the source files.)

Table A1. Photometric properties of spectroscopic sample

Target (1)	R.A. (2)	Decl. (3)	$F_{1.4 \text{ GHz}}$ (4)	g (5)	r (6)	r'_{syn} (7)	W_1 (8)	W_2 (9)	W_3 (10)	$W_1 - W_2$ (11)	$W_2 - W_3$ (12)
MALS0017–1256	00:17:08.03	−12:56:24.9	929.7	20.47	19.72	20.0	14.16	12.96	9.51	1.20	3.44
MALS0022+0608	00:22:32.46	+06:08:04.6	339.7	18.99	18.54	18.5	13.23	12.21	9.03	1.02	3.18
MALS0042+1246	00:42:43.06	+12:46:57.6	635.0	20.15	19.93	20.4	15.78	14.54	11.13	1.24	3.41
MALS0051+1747	00:51:47.15	+17:47:10.3	1367.5	21.09	20.18	20.5	15.59	14.65	11.42	0.93	3.23
MALS0053–0702	00:53:15.65	−07:02:33.4	248.2	20.89	20.22	20.3	16.31	15.25	11.95	1.06	3.30
MALS0105+1845	01:05:49.69	+18:45:07.1	339.5	20.32	19.86	19.4	15.61	14.81	11.66	0.80	3.15
MALS0117–0425	01:17:27.84	−04:25:11.5	421.4	20.91	20.71	20.2	16.05	15.00	11.71	1.06	3.29
MALS0211+1707	02:11:48.77	+17:07:23.2	539.8	20.64	20.76	20.4	16.22	15.42	11.82	0.80	3.60
MALS0216+1724	02:16:50.70	+17:24:04.9	395.2	20.75	20.29	19.9	15.99	15.09	11.91	0.90	3.18
MALS0226+0937	02:26:13.72	+09:37:26.3	374.6	18.4	15.03	14.11	10.74	0.92	3.37
MALS0226+1941	02:26:39.92	+19:41:10.1	209.8	21.0	16.52	15.46	11.90	1.06	3.56
MALS0240+0832	02:40:46.80	+08:32:58.3	305.4	19.6	15.57	14.59	11.49	0.97	3.10
MALS0249+0440	02:49:39.93	+04:40:28.9	420.5	20.55	20.18	20.6	16.15	15.10	11.68	1.05	3.42
MALS0249+1237	02:49:44.50	+12:37:06.3	261.2	17.5	15.03	14.35	11.16	0.68	3.19
MALS0256–0218	02:56:30.36	−02:18:44.5	260.3	19.17	18.79	18.8	15.21	13.88	10.27	1.33	3.61
MALS0304–1126	03:04:13.80	−11:26:53.5	335.0	20.3	16.98	15.84	12.34	1.14	3.50
MALS0314–0909	03:14:07.94	−09:09:46.9	226.8	20.4	15.25	14.61	11.72	0.64	2.89
MALS0317+0655	03:17:06.76	+06:55:50.3	211.8	22.29	21.90	20.6	14.78	14.12	11.13	0.66	2.99
MALS0328–0152	03:28:08.59	−01:52:20.2	221.9	18.5	15.46	14.55	11.31	0.91	3.24
MALS0341+1519	03:41:57.75	+15:19:25.5	200.4	21.40	21.02	21.2	16.32	15.22	11.77	1.09	3.45
MALS0350–0351	03:50:16.86	−03:51:11.3	230.5	19.2	15.21	14.00	10.65	1.21	3.35
MALS0356+1900	03:56:33.46	+19:00:34.6	1051.3	19.89	19.51	20.0	15.76	14.95	11.73	0.80	3.22
MALS0356–0831	03:56:34.55	−08:31:21.3	239.7	21.0	16.52	15.34	11.84	1.18	3.50
MALS0455+1850	04:55:41.91	+18:50:10.9	328.1	20.8	14.61	13.86	10.79	0.75	3.07
MALS0510–1959	05:10:24.23	−19:59:50.3	336.2	20.4	14.95	14.15	11.16	0.79	2.99
MALS0512+1517	05:12:40.99	+15:17:23.8	966.5	20.23	19.58	19.4	15.53	14.45	10.99	1.08	3.46
MALS0516+0732	05:16:56.35	+07:32:52.7	231.7	17.1	14.18	13.53	10.65	0.65	2.87
MALS0519+1746	05:19:38.34	+17:46:41.2	319.1	20.61	19.76	19.8	16.73	16.03	12.11	0.70	3.92
MALS0529–1126	05:29:05.55	−11:26:07.5	455.8	20.1	14.99	14.30	11.30	0.69	3.00
MALS0600–0710	06:00:12.92	−07:10:37.9	224.9	20.6	16.14	15.28	12.22	0.86	3.06
MALS0730+1739	07:30:37.09	+17:39:51.5	694.2	23.84	22.34	22.8	16.91	16.13	12.07	0.78	4.06
MALS0731+1433	07:31:59.01	+14:33:36.3	316.5	18.60	18.46	18.4	15.49	14.76	11.01	0.73	3.75
MALS0824–1029	08:24:44.81	−10:29:43.6	345.4	18.4	15.42	14.70	11.28	0.71	3.42
MALS0836+0406	08:36:01.35	+04:06:36.0	435.3	22.30	20.95	22.4	15.52	14.91	11.86	0.60	3.05
MALS0845–1118	08:45:48.34	−11:18:00.1	264.4	16.18	15.29	12.03	0.89	3.25
MALS0909–1637	09:09:10.66	−16:37:53.8	340.1	20.1	15.87	15.20	11.84	0.67	3.36
MALS0909–0500	09:09:16.99	−05:00:53.2	457.2	21.1	15.68	15.00	11.75	0.68	3.25
MALS0910–0526	09:10:51.01	−05:26:26.8	337.9	17.8	14.57	13.61	10.46	0.96	3.16
MALS0939–1731	09:39:19.21	−17:31:35.4	263.3	20.4	15.19	14.07	10.67	1.12	3.40
MALS0941–0321	09:41:46.01	−03:21:21.7	346.2	21.2	16.59	15.77	11.94	0.82	3.83
MALS0951–0601	09:51:38.34	−06:01:38.0	378.8	20.5	16.27	15.46	11.95	0.82	3.50

Table A1 continued

Table A1 (*continued*)

Target (1)	R.A. (2)	Decl. (3)	F _{1.4 GHz} (4)	<i>g</i> (5)	<i>r</i> (6)	<i>r'</i> _{syn} (7)	<i>W</i> ₁ (8)	<i>W</i> ₂ (9)	<i>W</i> ₃ (10)	<i>W</i> ₁ − <i>W</i> ₂ (11)	<i>W</i> ₂ − <i>W</i> ₃ (12)
MALS0954+1252	09:54:14.75	+12:52:22.6	355.7	16.95	15.74	11.79	1.21	3.95
MALS1007−1817	10:07:43.51	−18:17:32.4	205.2	21.0	14.96	14.22	10.16	0.74	4.06
MALS1008−0959	10:08:02.27	−09:59:19.3	645.3	19.6	15.70	14.55	11.24	1.15	3.31
MALS1009+1602	10:09:54.53	+16:02:03.8	201.9	20.81	20.64	20.6	16.09	15.18	11.57	0.91	3.61
MALS1024−0852	10:24:44.61	−08:52:06.4	463.8	21.4	16.36	15.58	12.51	0.78	3.07
MALS1033−1210	10:33:35.61	−12:10:32.1	2065.1	20.9	16.59	15.80	11.70	0.80	4.10
MALS1043+1641	10:43:47.34	+16:41:06.9	259.1	22.15	20.52	21.3	15.82	15.19	11.74	0.63	3.45
MALS1046+1535	10:46:08.12	+15:35:36.6	430.9	22.1	16.83	16.03	11.88	0.80	4.15
MALS1050−0318	10:50:24.43	−03:18:08.8	243.5	18.74	18.70	18.6	15.25	14.06	10.77	1.19	3.29
MALS1059−1118	10:59:55.36	−11:18:18.7	314.5	20.6	16.60	15.71	12.18	0.89	3.53
MALS1119−0527	11:19:17.36	−05:27:07.9	1174.4	20.6	16.58	15.94	11.65	0.64	4.29
MALS1124−1501	11:24:02.56	−15:01:59.1	261.9	19.3	16.65	15.77	11.87	0.88	3.90
MALS1130−1006	11:30:15.25	−10:06:38.4	215.2	16.26	15.50	12.00	0.76	3.51
MALS1148+1404	11:48:25.45	+14:04:49.7	322.0	22.89	21.66	22.6	16.27	15.61	11.79	0.67	3.82
MALS1150+1317	11:50:43.70	+13:17:36.1	254.4	20.12	19.88	19.7	16.31	15.24	12.02	1.07	3.22
MALS1206−0714	12:06:32.23	−07:14:52.6	698.8	20.5	16.03	15.41	11.68	0.62	3.73
MALS1215−0628	12:15:14.42	−06:28:03.5	360.4	19.8	15.78	15.01	11.76	0.76	3.26
MALS1218−0631	12:18:36.18	−06:31:15.8	409.1	18.9	14.35	13.50	10.41	0.85	3.09
MALS1219−1809	12:19:05.45	−18:09:11.2	300.3	19.5	14.80	14.15	11.26	0.65	2.89
MALS1221−1237	12:21:23.49	−12:37:24.1	343.7	20.1	15.67	14.79	11.77	0.88	3.02
MALS1225−1144	12:25:24.48	−11:44:31.2	479.5	20.9	14.90	14.26	11.24	0.64	3.03
MALS1231−1236	12:31:50.30	−12:36:37.5	276.0	19.2	15.00	13.86	10.42	1.14	3.44
MALS1318−1441	13:18:56.01	−14:41:55.0	283.0	19.8	15.14	14.08	10.67	1.05	3.42
MALS1343−0834	13:43:09.26	−08:34:57.5	241.5	19.8	15.93	15.09	11.88	0.84	3.21
MALS1351−1019	13:51:31.98	−10:19:32.9	726.1	19.3	15.02	14.12	10.74	0.90	3.38
MALS1456+0456	14:56:25.83	+04:56:45.2	287.9	20.63	20.29	20.5	16.21	15.50	12.62	0.71	2.88
MALS1623+1239	16:23:03.03	+12:39:58.4	523.3	18.60	18.23	18.1	16.16	15.50	12.16	0.66	3.34
MALS1625−0416	16:25:39.34	−04:16:16.3	257.2	23.05	22.69	19.1	16.39	15.75	12.47	0.64	3.28
MALS1639+1144	16:39:06.46	+11:44:09.2	341.9	20.72	19.62	19.6	16.17	15.13	11.48	1.03	3.66
MALS1645−0432	16:45:52.10	−04:32:53.3	423.3	20.7	16.78	15.94	12.32	0.84	3.62
MALS1649+0626	16:49:50.51	+06:26:53.3	389.2	18.6	14.75	13.64	10.40	1.11	3.23
MALS1650−1248	16:50:38.03	−12:48:54.5	275.5	20.8	16.23	15.07	11.27	1.17	3.79
MALS1653−0102	16:53:57.67	−01:02:14.2	317.4	21.27	20.47	20.4	15.71	14.80	11.67	0.91	3.13
MALS1716−0613	17:16:27.09	−06:13:56.5	229.9	19.4	14.03	12.82	9.49	1.21	3.33
MALS1721+1626	17:21:05.79	+16:26:49.1	507.9	19.3	16.11	15.31	11.80	0.79	3.51
MALS1722+1652	17:22:39.45	+16:52:08.7	257.1	19.9	16.29	15.50	12.31	0.80	3.19
MALS1724+0326	17:24:23.07	+03:26:32.5	217.8	18.7	16.31	15.23	11.61	1.08	3.62
MALS1725+0622	17:25:07.45	+06:22:42.1	213.4	18.6	15.40	14.49	11.36	0.91	3.14
MALS2034−0523	20:34:25.65	−05:23:32.2	419.7	18.6	15.58	14.61	11.18	0.97	3.43
MALS2054−0932	20:54:56.08	−09:32:40.8	313.6	20.8	16.42	15.44	11.74	0.98	3.70
MALS2059−1440	20:59:59.61	−14:40:43.1	1018.1	21.2	14.63	13.63	10.45	0.99	3.18
MALS2120+1327	21:20:42.48	+13:27:24.2	401.5	20.02	19.56	19.5	14.68	13.91	10.56	0.77	3.35

Table A1 *continued*

Table A1 (*continued*)

Target (1)	R.A. (2)	Decl. (3)	$F_{1.4 \text{ GHz}}$ (4)	g (5)	r (6)	r'_{syn} (7)	W_1 (8)	W_2 (9)	W_3 (10)	$W_1 - W_2$ (11)	$W_2 - W_3$ (12)
MALS2139+1718	21:39:37.03	+17:18:26.9	219.4	19.26	19.06	18.9	15.43	14.23	10.88	1.21	3.34
MALS2158+0925	21:58:00.88	+09:25:46.4	437.7	21.01	19.78	20.5	15.19	14.33	9.91	0.87	4.41
MALS2201+0312	22:01:27.50	+03:12:15.6	300.5	23.58	22.75	20.3	16.31	15.61	11.78	0.70	3.83
MALS2220+1307	22:20:04.97	+13:07:12.1	812.0	20.46	20.16	20.4	14.94	14.19	11.11	0.74	3.08
MALS2223+1213	22:23:59.11	+12:13:38.9	246.4	21.70	20.40	21.5	15.05	13.99	10.76	1.06	3.23
MALS2224+1304	22:24:20.03	+13:04:50.2	294.5	20.91	20.62	20.8	16.15	15.13	11.67	1.02	3.46
MALS2230+0348	22:30:50.19	+03:48:36.8	242.8	22.48	21.79	22.9	16.53	15.92	12.15	0.61	3.77
MALS2238-1344	22:38:26.48	-13:44:22.6	241.2	20.0	14.78	13.97	10.78	0.81	3.19
MALS2243+1814	22:43:54.81	+18:14:45.9	1004.4	20.98	20.23	20.8	15.94	14.48	10.34	1.47	4.13
MALS2247+1211	22:47:05.52	+12:11:51.4	223.7	18.2	17.27	16.66	12.25	0.61	4.41
MALS2258-0958	22:58:13.47	-09:58:17.2	225.7	25.59	26.20	...	17.37	16.52	12.19	0.84	4.34
MALS2300+1940	23:00:36.41	+19:40:02.9	210.4	19.54	19.48	19.6	15.94	15.22	12.19	0.72	3.03
MALS2300+0337	23:00:40.87	+03:37:10.3	509.0	19.68	19.60	19.9	15.54	14.45	10.89	1.09	3.56
MALS2308-1149	23:08:05.25	-11:49:45.7	256.8	20.0	16.66	15.90	12.07	0.77	3.82
MALS2310+1114	23:10:02.89	+11:14:03.6	248.1	19.95	19.82	20.0	16.55	15.39	12.12	1.16	3.27
MALS2316+0429	23:16:34.61	+04:29:40.2	214.0	19.09	18.97	19.2	15.72	14.46	11.15	1.26	3.31
MALS2332-1423	23:32:31.61	-14:23:18.8	234.1	20.5	14.79	14.10	11.06	0.68	3.04
MALS2338-1218	23:38:08.04	-12:18:51.4	450.9	19.6	16.01	15.04	11.81	0.97	3.23
MALS2340+0959	23:40:07.26	+09:59:59.0	205.0	21.89	21.63	22.6	15.42	14.81	11.95	0.62	2.86
MALS2359+1924	23:59:14.02	+19:24:20.6	284.1	21.45	20.67	20.8	14.46	13.58	10.18	0.88	3.40

NOTE— (1) Target identifier; (2) Right Ascension (epoch J2000); (3) Declination (epoch J2000);
(4) Flux at 1.4 GHz in mJy; (5) SDSS g -band AB magnitude; (6) SDSS r -band AB magnitude;
(7) Synthetic SDSS r -band magnitude calculated from the observed spectrum (typical uncertainty of ± 0.2 mag);
(8)–(10) *WISE* bands 1, 2 and 3 at 3.4, 4.6, and 12 μm in Vega magnitudes;
(11)–(12) *WISE* colors in Vega magnitudes.